AN INVERSE-DIRECT HYBRID NAVIER-STOKES SOLVER USING PSEUDE-ANALYTIC FUNCTIONS

By

Teruo Miyazaki
Department of Mechanical Engineering, Kokushikan University,
4-28-1, Setagaya, Setagaya-ku, Tokyo 154 , Japan

An inverse-direct hybrid Navier-Stokes solver using pseudo-analytic function theories, which can deal with numerous parameters and variables appearing in the unsteady three-dimensional compressible viscous solvers, is presented. Thanks to the pseudo-analytic function theory, the integral operators of direct solvers were defined along the physical boundaries besides inlet and outlet boundaries and they can simply integrate with the inverse method. An interchange of necessary informations between direct and inverse methods can be smoothly and sufficiently excuted without any artificial technique. The application of present method to a conventional blade designing is very easy and can be done completely. In the present paper the inverse method demonstrates the ideal cases in which the data are supposed to be known exactly and complete. Using the calculated results for the unsteady inlet transonic rotor flow and the linear cascade flows with and without air-injection, the numerical examples to reconstruct the blade suction surfaces were successfully given. The stabilities in inverse computations for both cases were very good and the code proved useful for the cases.

Introduction

The need for engineering design of turbomachines with high performance and structual durability of blade rows has motivated engineers to develop an inverse method, which accounts for unsteady, three-dimensional, compressible, and viscous effects. From an engineering point of view numerous parameters and variables appearing in governing field equations with arbitrary boundary conditions might be the objectives of everyday designing. It is well-known that inverse modelling ordinarily involves the estimation of the solution of an equation from a set of observed data. In practice, we can measure only the function of data and not derivatives and observational errors cannot be completely avoided. Then many equations of the first kind for the current problems under consideration are ill-posed and may certainly yield some difficulties. Even the unsteady three-dimensional compressible Navier-Stokes equation can only represent an aspect of flow phenomena. Coarsely simplified flow models or the discretized differential equations lead to intrinsic ambiguities.i.e., different values of the parameters in the governing equations can meet the same measured or designed values and any errors act as a perturbation on the equation. Detailed elucidation on the given or design data is essential. To reduce these ambiguities in the solution which are unstable the results of experience accumulated by engineers and scientists are inevitable. Apparently, such incorporation only, may not improve the situation, bacause that the governing equations might be nonlinear. While in the ideal case when the data are supposed to be known exactly and complete (the perfect data), it might be thought that an exact solution to an inverse problem would prove also useful for the practical case and only the questions of existence, uniqueness, stability and construction of the solution would be of great importance in testing the assumption behind any mathematical model. However, when solving inverse problems numerically, the solution obtained by analytic formula is usually very sensitive to the way in which the data set is completed and to errors in it.

The main objective of the present paper is to discuss the information content of the governing equation that certain coefficients or the variable terms or functionals of these coefficients or the variable terms inaccessible to measurement can be determined in as stable and unique manner. Owing to the pseudo-analytic function theories, the existing direct solvers with integral operators for the unsteady three-dimensional compressible viscous cascade flows[(1)-(4)] can be applied to transonic flowfields with unsteady inlet conditions. Body-fitted coordinates were naturally employed. Three different kinds of computation surfaces, blade-to-blade, meridional and cross-sectional ones those allow any deflections were introduced. The direct solvers gives the numerical results through the iterative process and the incorporation with an inverse solution can be easily achieved. Now the current inverse method uses *a line integral and a successive iteration and* is shown especially for the cases of reconstruction of profile shapes from the velocity or temperature distributions. The inverse-direct hybrid method is also applicable to the cases for setting of inlet flow conditions to meet a required performance and for the considerations of inflow conditions in film-cooling problems. the admissible order of disturbance level at the inlet, the permissible order of inlet boundary layer thickness to maintain the suitable cascade performance. and so on. The theoretical concepts such as quasi-conformal mappings and the other conventional mappings may play important roles in the present method. The present background of the theoretical method may guarantee the convergence of the numerical computation without sophisticated numerical optimization techniques or a cut and try approach. The discussed scheme here and the given numerical examples both may show that a variety of future applications of the current method are promising.

Analysis

Principle of the Solution

Various types of inverse or design methods have been ordinarily proposed to provide geometries of cascades corresponding to a set of observed or imposed data such as given blade surface velocity or pressure distributions with geometric constraints. Then, the solutions of the governing equations for such inverse problems of interest are inevitablly ill-posed. Under the existence of strong shocks, on the other hand, the numerous parameters and variable terms inaccessible to measurement appearing in the unsteady three-dimensional compressible viscous flow governing equations are objectives of eveyday designings of turbomachines with high performance and structual durability. A practical inverse or design solution, from the engineering point of view, should offer numerical methods which can determine these parameters and variable terms in as stable and unique manner. Now a priori adequate informations may naturally reduce the ambiguities pointed out in the inverse solutions. To stress on such informations, the main object of present study is concentrated on the ideal case with the perfect data. After integrating with the direct solvers, necessary and sufficient informations for the inverse method can be afforded. The present method also proves useful for the practical cases mentioned above. Taking into account the entropy variation through shocks, the present inverse technique uses the unsteady three-dimensional compressible Navier-Stokes solvers[(1)-(4)].In addition to the foregoing field equations, boundary conditions must be specified at the blade surfaces and at the inflow and outflow boundaries. For viscous flow simulations, a non-slip condition and a prescribed heat flux or wall temperature distribution are enforced along the blade wall surfaces.

Governing Equations for Unsteady Three-Dimensional Compressible Viscous Flows

For the practical inverse or design problems in engineerings, the governing equations should represent the possible flow phenomena in general. The present inverse method uses the governing equations for the unsteady three-dimensional compressible viscous cascade flow with the arbitrary inlet and wall boundary conditions[(1)-(4)] written in the blade relative frame. Those are the continuity, momentum, energy, and diffusion equations, besides additional aerothermodynamic relations which shall be introduced, according to the objective of designing. Using the cylindrical coordinates (x, ϕ , r) and the corresponding velocity components(W_x , W_ϕ , W_r),the governing equations are written as follows. The continuity equation is such that:

$$\frac{\partial \log\rho}{\partial t}+\frac{\partial W_x}{\partial x}+\frac{1}{r}\frac{\partial W_\phi}{\partial \phi}+\frac{\partial W_r}{\partial r}+\frac{W_r}{r}$$
$$+W_x\frac{\partial \log\rho}{\partial x}+W_\phi\frac{1}{r}\frac{\partial \log\rho}{\partial \phi}+W_r\frac{\partial \log\rho}{\partial r}=0 \quad (1)$$

The momentum equations in axial, circumferential,and radial directions are such that:

$$\frac{\partial W_x}{\partial t}+W_\phi\left(\frac{1}{r}\frac{\partial W_x}{\partial \phi}-\frac{\partial W_\phi}{\partial x}\right)$$
$$-W_r\left(\frac{\partial W_r}{\partial x}-\frac{\partial W_x}{\partial r}\right)=-\frac{\partial I}{\partial x}+T\frac{\partial s}{\partial x}$$
$$+\frac{1}{3}\frac{\mu+2\mu_B}{\rho}\frac{\partial \Delta}{\partial x}+\frac{\mu}{\rho}\nabla^2 W_x+V_{s,x} \quad (2)$$

$$\frac{\partial W_\phi}{\partial t}-W_x\left(\frac{1}{r}\frac{\partial W_x}{\partial \phi}-\frac{\partial W_\phi}{\partial x}\right)$$
$$+W_r\left(\frac{\partial W_\phi}{\partial r}-\frac{1}{r}\frac{\partial W_r}{\partial \phi}\right)+\frac{W_r W_\phi}{r}+2\omega W_r$$
$$=-\frac{1}{r}\frac{\partial I}{\partial \phi}+\frac{T}{r}\frac{\partial s}{\partial \phi}+\frac{1}{3}\frac{\mu+2\mu_B}{\rho}\frac{1}{r}\frac{\partial \Delta}{\partial \phi}$$
$$+\frac{\mu}{\rho}\left(\nabla^2 W_\phi+\frac{2}{r^2}\frac{\partial W_r}{\partial \phi}-\frac{W_\phi}{r^2}\right)+V_{s,\phi} \quad (3)$$

$$\frac{\partial W_r}{\partial t} - W_\phi \left(\frac{\partial W_\phi}{\partial r} - \frac{1}{r}\frac{\partial W_r}{\partial \phi} \right) + W_x \left(\frac{\partial W_r}{\partial x} - \frac{\partial W_x}{\partial r} \right) - \frac{W_\phi^2}{r} - 2\omega W_\phi = -\frac{\partial I}{\partial r} + T\frac{\partial s}{\partial r} + \frac{1}{3}\frac{\mu + 2\mu_B}{\rho}\frac{\partial \Delta}{\partial r} + \frac{\mu}{\rho}\left(\nabla^2 W_r - 2\frac{1}{r^2}\frac{\partial W_\phi}{\partial \phi} - \frac{W_r}{r^2} \right) + V_{s,r} \tag{4}$$

where

$$\nabla^2 = \frac{\partial^2}{\partial x^2} + \frac{1}{r^2}\frac{\partial^2}{\partial \phi^2} + \frac{\partial^2}{\partial r^2} + \frac{1}{r}\frac{\partial}{\partial r} \tag{5}$$

$$\Delta = \frac{\partial W_x}{\partial x} + \frac{1}{r}\frac{\partial W_\phi}{\partial \phi} + \frac{\partial W_r}{\partial r} + \frac{W_r}{r} \tag{6}$$

$$V_{s,x} = \frac{1}{\rho}\left\{ 2\frac{\partial \mu}{\partial x}\frac{\partial W_x}{\partial x} - \frac{2}{3}\frac{\partial(\mu - \mu_B)}{\partial x}\Delta + \frac{1}{r}\frac{\partial \mu}{\partial \phi}\left(\frac{\partial W_\phi}{\partial x} + \frac{1}{r}\frac{\partial W_x}{\partial \phi} \right) + \frac{\partial \mu}{\partial r}\left(\frac{\partial W_r}{\partial x} + \frac{\partial W_x}{\partial r} \right) \right\} \tag{7}$$

$$V_{s,\phi} = \frac{1}{\rho}\left\{ 2\frac{1}{r}\frac{\partial \mu}{\partial \phi}\left(\frac{1}{r}\frac{\partial W_\phi}{\partial \phi} + \frac{W_r}{r} \right) - \frac{2}{3}\frac{1}{r}\frac{\partial(\mu - \mu_B)}{\partial \phi}\Delta + \frac{\partial \mu}{\partial r}\left(\frac{1}{r}\frac{\partial W_r}{\partial \phi} + \frac{\partial W_\phi}{\partial r} - \frac{W_\phi}{r} \right) + \frac{\partial \mu}{\partial x}\left(\frac{\partial W_\phi}{\partial x} + \frac{1}{r}\frac{\partial W_x}{\partial \phi} \right) \right\} \tag{8}$$

$$V_{s,r} = \frac{1}{\rho}\left\{ 2\frac{\partial \mu}{\partial r}\frac{\partial W_r}{\partial r} - \frac{2}{3}\frac{\partial(\mu - \mu_B)}{\partial r}\Delta + \frac{\partial \mu}{\partial x}\left(\frac{\partial W_x}{\partial r} + \frac{\partial W_r}{\partial x} \right) + \frac{1}{r}\frac{\partial \mu}{\partial \phi}\left(\frac{1}{r}\frac{\partial W_r}{\partial \phi} + \frac{\partial W_\phi}{\partial r} - \frac{W_\phi}{r} \right) \right\} \tag{9}$$

Also the energy equation is such that:

$$\frac{\partial^2 T}{\partial x^2} + \frac{1}{r^2}\frac{\partial^2 T}{\partial \phi^2} + \frac{\partial^2 T}{\partial r^2} + \left(\frac{1}{\kappa}\frac{\partial \kappa}{\partial x} - \frac{\rho \hat{C}_v}{\kappa}W_x \right)\frac{\partial T}{\partial x} + \left(\frac{1}{\kappa}\frac{1}{r}\frac{\partial \kappa}{\partial \phi} - \frac{\rho \hat{C}_v}{\kappa}W_\phi \right)\frac{1}{r}\frac{\partial T}{\partial \phi} + \left(\frac{1}{r} + \frac{1}{\kappa}\frac{\partial \kappa}{\partial r} - \frac{\rho \hat{C}_v}{\kappa}W_r \right)\frac{\partial T}{\partial r} - \frac{1}{\kappa}\Psi_v + \frac{\rho \hat{C}_v}{\kappa}\frac{\partial T}{\partial t} = 0 \tag{10}$$

where

$$\Psi_v = 2\mu\Bigg[\left(\frac{\partial W_x}{\partial x} \right)^2 + \left\{ \frac{1}{r}\left(\frac{\partial W_\phi}{\partial \phi} + W_r \right) \right\}^2 + \left(\frac{\partial W_r}{\partial r} \right)^2 + 2\left(\frac{\partial W_\phi}{\partial x} + \frac{1}{r}\frac{\partial W_x}{\partial \phi} \right)^2 + 2\left\{ \frac{1}{r}\frac{\partial W_r}{\partial \phi} + r\frac{\partial}{\partial r}\left(\frac{W_\phi}{r} \right) \right\}^2 + 2\left(\frac{\partial W_x}{\partial r} + \frac{\partial W_r}{\partial x} \right)^2 \Bigg] + \left(\mu_B - \frac{2}{3}\mu \right)\left(\nabla \cdot \vec{W} \right)^2 \tag{11}$$

Here the notations, W , ρ , μ, μ_B , ω , I , T , s , $\hat{C}_V$, and q , indicate the relative velocity, the density, the viscosity, the bulk viscosity, the angular velocity of blades, the rothalpy, temperature, the entropy per unit mass, the heat capacity of the fluid at constant volume, per unit mass, and the energy flux, respectively. The inverse solutions for the equations hitherto mentioned are common to axial-, radial- and mixed-flow types of turbomachines. Therefore, the discussions hereafter, refer only for the axial-flow type. Under the governing equations there are no particular restrictions on boundary conditions in the present solution. Arbitrary unsteady and non-uniform inlet and outlet flow conditions and various types of wall conditions such as with or without air-injection or with designed temperature distributions and so on, are, of course, allowed in the solution. For an abbreviated description here the diffusion equation and the other aerothermodynamic relations for respective flowfields, are not referred to.

Introduction of Complex Coordinates and Velocities

We obtain complex forms of the given equations cited above through complex coordinates and complex velocities as follows.
Complex coordinates:

$$z_n = \xi_n + i\eta_n, \tag{12}$$

$$\zeta_n = \xi_n - i\eta_n, \tag{13}$$

$$(n = 1, 2, 3)$$

with

$$\xi_1 = x, \ \eta_1 = \int r\, d\phi; \ \ \xi_2 = x_1, \ \eta_2 = r;$$

$$\xi_3 = \int r\,d\phi,\ \eta_3 = r$$

Complex velocities:

$$w_1 = W_x - iW_\phi, \quad \overline{w_1} = W_x + iW_\phi; \tag{14}$$
$$w_2 = W_x - iW_r, \quad \overline{w_2} = W_x + iW_r; \tag{15}$$
$$w_3 = W_\phi - iW_r, \quad \overline{w_3} = W_\phi + iW_r \tag{16}$$

In the above definitions subfix n stands for the three different kinds of computation surfaces. Also we use derivatives with respect to z_n and ζ_n such that :

$$\frac{\partial}{\partial z_n} = \frac{1}{2}\left(\frac{\partial}{\partial \xi_n} - i\frac{\partial}{\partial \eta_n}\right), \tag{17}$$
$$\frac{\partial}{\partial \zeta_n} = \frac{1}{2}\left(\frac{\partial}{\partial \xi_n} + i\frac{\partial}{\partial \eta_n}\right), \tag{18}$$
$$\frac{\partial^2}{\partial z_n \partial \zeta_n} = \frac{1}{4}\left(\frac{\partial^2}{\partial \xi_n^2} + \frac{\partial^2}{\partial \eta_n^2}\right), \tag{19}$$
$$(n = 1, 2, 3)$$

Fundamental Equations in Complex Forms

Using the definitions shown above, the governing equations are reduced to as follows [(1)-(4)] .
The fundamental equation for the comlex velocity w_n is such that :

$$\frac{\partial^2 w_n(z_n, \zeta_n, t)}{\partial z_n \partial \zeta_n} + A_{n,2}(z_n, \zeta_n, t)\frac{\partial w_n}{\partial z_n}$$
$$+B_{n,2}(z_n, \zeta_n, t)\frac{\partial w_n}{\partial \zeta_n} + C_{n,2}(z_n, \zeta_n, t)\, w_n$$
$$+D_{n,2}(z_n, \zeta_n, t)\,\overline{w_n} + F_n(z_n, \zeta_n, t)$$
$$+E\frac{\partial w_n}{\partial t} = 0\ ,\ (n = 1, 2, 3) \tag{20}$$

Also the reduced equation of energy is such that :

$$\frac{\partial^2 T}{\partial z_n \partial \zeta_n} + A_n^E(z_n, \zeta_n, t)\frac{\partial T}{\partial z_n}$$
$$+B_n^E(z_n, \zeta_n, t)\frac{\partial T}{\partial \zeta_n} + F_n^E(z_n, \zeta_n, t)$$
$$+E_n^E(z_n, \zeta_n, t)\frac{\partial T}{\partial t} = 0$$
$$(n = 1, 2, 3) \tag{21}$$

On the direct solutions using the pseudo-analytic function theories the unsteady three-dimensional compressible Navier-Stokes solvers with integral operators, which can be applied to transonic flowfields with unsteady inlet conditions and a high degree of geomeyric complexity were already presented[(1)-(4)]. The operators were defined for initial boundary value problems[(5),(6)]. The direct solvers gives the results through the iterative process and the integration can be easily achieved.

Reduction of Fundamental Equations on Solid Boundaries for Non-Slip Flows

On solid boundaries the velocity distributions in the relative frame are zero or constant, except at sinks or sources. The fundamental equations for the comlex velocity w_n at each time increments are then reduced to such that :

$$\frac{\partial^2 w_n(z_n, \zeta_n; t)}{\partial z_n \partial \zeta_n} + A_{n,2}^0(z_n, \zeta_n; t)\frac{\partial w_n}{\partial z_n}$$
$$+B_{n,2}^0(z_n, \zeta_n; t)\frac{\partial w_n}{\partial \zeta_n} + F_n^0(z_n, \zeta_n; t) = 0 \tag{22}$$
$$w_n(z_n, \zeta_n; t) = w_n^0 \mid_{\ t=t} \tag{23}$$
$$(n = 1, 2, 3)$$

In cace of $w_n^0 = 0$, the coefficients, $A_{n,2}^0$, $B_{n,2}^0$ and $F_{n,2}^0$ are as follows.

For the blade-to-blade surfaces

$$A_{1,2}^0 = B_{1,2}^0 = 0, \tag{24}$$
$$F_1^0 = \frac{1}{4}\frac{\partial^2 w_1}{\partial r^2} + \frac{1}{4}\frac{\partial w_1}{\partial r} + \frac{1}{6}\frac{\mu + 2\mu_B}{\mu}\frac{\partial \Delta'}{\partial z_1}$$
$$-i\frac{1}{2}\frac{1}{r^2}\frac{\partial W_r}{\partial \phi} - \frac{1}{2}\frac{\rho}{\mu}\left(\frac{\partial I}{\partial z_1} - T\frac{\partial s}{\partial z_1}\right)$$
$$+\frac{1}{4}\left(V'_{s,x} - iV'_{s,\phi}\right) \tag{25}$$

for the meridional surfaces

$$A_{2,2}^0 = -B_{2,2}^0 = i\frac{1}{4r} \tag{26}$$
$$F_2^0 = +\frac{1}{4}\frac{1}{r^2}\frac{\partial^2 w_2}{\partial \phi^2} + \frac{1}{6}\frac{\mu + 2\mu_B}{\mu}\frac{\partial \Delta'}{\partial z_2}$$
$$+i\frac{1}{2}\frac{1}{r^2}\frac{\partial W_\phi}{\partial \phi} - \frac{1}{2}\frac{\rho}{\mu}\left(\frac{\partial I}{\partial z_2} - T\frac{\partial s}{\partial z_2}\right)$$
$$+\frac{1}{4}\left(V'_{s,x} - iV'_{s,r}\right) \tag{27}$$

and for the cross-sectional surfaces

$$A_{2,3}^0 = i\frac{3}{4}\frac{1}{r},\ B_{2,3}^0 = i\frac{1}{4}\frac{1}{r} \tag{28}$$
$$F_3^0 = \frac{1}{4}\frac{\partial^2 w_3}{\partial x^2} + \frac{1}{6}\frac{\mu + 2\mu_B}{\mu}\frac{\partial \Delta'}{\partial z_3}$$
$$-\frac{1}{2}\frac{\rho}{\mu}\left(\frac{\partial I}{\partial z_3} - T\frac{\partial s}{\partial z_3}\right) + \frac{1}{4}\left(V'_{s,\phi} - iV'_{s,r}\right) \tag{29}$$

Similarly the fundamental equation of energy is written such that :

$$\frac{\partial^2 T}{\partial z_n \partial \zeta_n} + A_n^{E,0}(z_n, \zeta_n; t)\frac{\partial T}{\partial z_n}$$
$$+B_n^{E,0}(z_n, \zeta_n; t)\frac{\partial T}{\partial \zeta_n} + F_n^{E,0}(z_n, \zeta_n; t)$$
$$+E_n^{E,0}(z_n, \zeta_n; t)\frac{\partial T}{\partial t} = 0\ \ (n = 1, 2, 3) \tag{30}$$

The variable coefficients in the above equation is omitted.

Numerical Procedures

The information content of the governing equation naturally dominates the stability and uniqueness in the designing. Discussions for a range of plausible and reasonable solutions in solving ill-posed flow problems numerically, are unavoidable. Moreover, the other various questions remain unsolved. Instead of the general discussion of existence, uniqueness, stability and construction in a complete solution of inverse or design problems, here, only usefulness of an exact solution to an inverse problem with perfect data shall be demonstrated for the practical cases. As was mentioned, ambiguities in the inverse solutions can be reduced by incorporating of a priori informations. Fig. 1 shows the present scheme for designing of three-dimensional high approach Mach number rotor blade contours, as an example of inverse or design method. The boundary condition on blade wall surfaces itself is the objective of the current inverse problems.

Computation Surfaces and Paths

For the integration of the inverse solution with the direct ones[(1)-(4)] the present solver uses three different kinds of computation surfaces, blade-to-blade, meridional and cross-sectional ones those allow any deflections as shown in Fig. 2. The current inverse method likewise the direct methods uses the integral representation with body-fitted coordinates and can fix the solution through the iteration.The figure also indicates the computation paths on these surfaves. The details of computation paths on a blade-to-blade are shown in Fig. 3. The solid and broken lines in the figure indicate the computation paths for the direct and the inverse solver, respectively. In the numerical calculation, portions of both computation paths not including reference points to be designed coincide with each other. The usual design factors, the velocity distribution on blade suction surface determining the gas dynamic performance and the thickness distribution which determines the performance of the vibration and strength of blade, are the current objectives. Then the numerical method is applied to the cases of reconstruction of profile contours from the velocity or temperature distributions on the blades. In the blade passages several cross-sectional surfaces are employed.

Correction of Blade Coordinates

Introducing the pseudo-analytic function theories [(1)-(4)], variety types of inverse problems can be done. As a conventional design problem. here, the method to give the unfixed blade coordinates, using velocity or pressure distributions on them, is shown as follows. After obtaining the velocity distributions, the blade coordinate can be written such that :

$$\begin{aligned}
&\left[z_n\left\{[w_n(s_n)]_{N+1}, \overline{[w_n(s_n)]_{N+1}}\right\}\right]_{N+1} \\
&= \left[z_n\left\{[w_n(s_{n,0})]_{N+1}, \overline{[w_n(s_{n,0})]_{N+1}}\right\}\right]_{N+1} \\
&\quad + \int_{s_{n,0}}^{s_n}\left\{\left[\frac{\partial z_n}{\partial w_n}\right]_{N+1}\cdot\left[\frac{dw_n}{ds_n}\right]_N \right. \\
&\quad \left. +\left[\frac{\partial z_n}{\partial \overline{w_n}}\right]_{N+1}\cdot\left[\frac{d\overline{w_n}}{ds_n}\right]_N\right\} ds_n \qquad (31)
\end{aligned}$$

where the formal derivatives :

$$\begin{aligned}
\frac{\partial z_n}{\partial w_n} &= \frac{1}{2}\cdot\left(\frac{\partial \xi_n}{\partial W_p} - \frac{\partial \eta_n}{\partial W_q}\right) \\
&\quad + \frac{i}{2}\cdot\left(\frac{\partial \eta_n}{\partial W_p} + \frac{\partial \xi_n}{\partial W_q}\right) \qquad (32) \\
\frac{\partial z_n}{\partial \overline{w_n}} &= \frac{1}{2}\cdot\left(\frac{\partial \xi_n}{\partial W_p} + \frac{\partial \eta_n}{\partial W_q}\right) \\
&\quad + \frac{i}{2}\cdot\left(\frac{\partial \eta_n}{\partial W_p} - \frac{\partial \xi_n}{\partial W_q}\right) \qquad (33)
\end{aligned}$$

with

$$w_n = W_p - i\cdot W_q \quad , \quad \overline{w_n} = W_p + i\cdot W_q$$
$$(n = 1,2,3 \ ; \ p\neq q, \quad p,q = x,\phi,r)$$

Subfix N in Eq.(31) indicates the iterative calculation on the whole flowfield. The reverse expression of formal derivative $\partial w_n/\partial z_n$ can be numerically obtained through the following iteratives process. In the first place the dependent variable w_n at each time increments in the fundamental equation (22) is changed such that :

$$\begin{aligned}
w_n(z_n,\zeta_n:t) &= \phi_n(z_n,\zeta_n:t) \\
&\quad \exp\left\{-\int_{\zeta_{n,0}}^{\zeta_n} A^0_{n,2}(z_n,\zeta'_n:t)d\zeta'_n\right\} \qquad (34)
\end{aligned}$$

Then the fundamental equation is reduced to such that :

$$\begin{aligned}
&\frac{\partial^2\phi_n}{\partial z_n\,\partial\zeta_n} + D^0_{n,2}(z_n,\zeta_n:t)\frac{\partial\phi_n}{\partial\zeta_n} \\
&\quad + F^T_n(z_n,\zeta_n:t) = 0 \qquad (35)
\end{aligned}$$

where

$$\begin{aligned}
&D^0_{n,2}(z_n,\zeta_n:t) \\
&= B^0_{n,2} - \int_{\zeta_{n,0}}^{\zeta_n}\frac{\partial A^0_{n,2}(z_n,\zeta'_n:t)}{\partial z_n}d\zeta'_n \qquad (36)
\end{aligned}$$

$$F_n^T(z_n,\zeta_n;t) = F_n^0 \exp\left\{\int_{\zeta_{n,0}}^{\zeta_n} A_{n,2}^0(z_n,\zeta_n';t)\,d\zeta_n'\right\} \quad (37)$$

After introducing an abbreviated notation

$$\Phi_n(\zeta_n;z_n) \equiv \frac{\partial o_n}{\partial z_n}\,. \quad (38)$$

Eq.(35) is rewritten such that :

$$\frac{\partial \Phi_n(\zeta_n;z_n)}{\partial \zeta_n} + D_{n,2}^0 \Phi_n(\zeta_n;z_n) + F_n^T = 0 \quad (39)$$

Here Φ_n can be given by a successive iteration as follows.

$$[\Phi_n]_{N+1,0} = [\Phi_n]_N \quad (40)$$

$$[\Phi_n]_{N+1,M+1} = [\Phi_n]_{N+1,M} + e^{[Q_n]_M} \int_{l_{n,0}}^{l_n} e^{-[Q_n]_M}\, F_n^T \left[\frac{d\zeta_n}{dl_n}\right]_{N+1,M} dl_1 \quad (41)$$

where

$$[Q_n]_M = \int_{l_{n,0}}^{l_n} [D_{n,2}^0]_M \left[\frac{d\zeta_n}{dl_n}\right]_{N+1,M} dl_1 \quad (42)$$

Now the formal derivative $\partial w_n/\partial z_n$ is obtained. The other formal derivative $\partial \overline{w_n}/\partial z_n$ can be similarly given through the conjugate form of fundamental equation such that:

$$\frac{\partial^2 \overline{w_n}(z_n,\zeta_n;t)}{\partial z_n\,\partial \zeta_n} + \overline{B_{n,2}^0}(z_n,\zeta_n;t)\frac{\partial \overline{w_n}}{\partial z_n} + \overline{A_{n,2}^0}(z_n,\zeta_n;t)\frac{\partial \overline{w_n}}{\partial \zeta_n} + \overline{F_n^0}(z_n,\zeta_n;t) = 0$$

$$(n = 1,2,3) \quad (43)$$

The reduced dependent variable is written such that:

$$\overline{w_n}(z_n,\zeta_n;t) = \psi_n(z_n,\zeta_n;t) \exp\left\{-\int_{\zeta_{n,0}}^{\zeta_n} \overline{B_{n,2}^0}(z_n,\zeta_n';t)\,d\zeta_n'\right\} \quad (44)$$

The values of derivatives $\partial w_n/\partial s_n$ and $\partial \overline{w_n}/\partial s_n$, remaining terms in Eq. (31), can be replaced by those for the direct solution given along the adjacent computation path, as shown in Fig. 3. After substituting these derivatives in Eq. (31), the unfixed blade coodinates can be finally assumed. Just in the same way as described above the temperature distribution can give the blade coordinates. The entropy and the other parameters in the governing equations can be deservedly utilized in the designing in much the same way as the velocity and temperature.

Fitting of Given Values in Arbitrary Locations

One may employ direct solvers in many design problems. In the direct solvers for initial boundary value problems[(1)-(4)], arbitrary boundary conditions at the inlet and outlet can be assigned to the control surfaces. Cross-sectional computation surfaces assumed as the control surfaces can be arranged at any axial location of the flowfield. The direct solutions were given using the integral representations. The pseudo-analytic function theory[(6)] yields a method of construction of solutions acquiring at arbitrary reference points in the flowfield some prescribed values. Through the reference points, therefore, we may set the velocity and temperature distributions together with the other aerothermodynamic parameters and variables, appearing in the governing equations, as follows[(1)].

For the velocity distribution:

$$\frac{\alpha}{2}[w_n(z_n,\zeta_n;t_j)]_{N+1} = \frac{\alpha}{2}[w_{n,i}(z_n;t_j)]_N + \frac{\alpha}{2}[\Phi_n(z_n,\zeta_n;t_j)]_N - \frac{1}{2\pi i}\oint_{G_n} \frac{[\Phi_n(z_n',\zeta_n';t_j)]_N}{z_n'-z_n} \left[1 - R_n\left(z_n', z_{n,1},\cdots,z_{n,m(n)}\right)\right] dz_n' \quad (45)$$

Also for the temperature distribution:

$$\frac{\alpha}{2}[T_n(z_n,\zeta_n;t_j)]_{N+1} = \frac{\alpha}{2}[T_{n,i}(z_n;t_j)]_N + \frac{\alpha}{2}[\Phi_n^E(z_n,\zeta_n;t_j)]_N - \frac{1}{2\pi i}\oint_{G_n} \frac{[\Phi_n^E(z_n',\zeta_n';t_j)]_N}{z_n'-z_n} \left[1 - R_n^E\left(z_n', z_{n,1},\cdots,z_{n,m(n)}\right)\right] dz_n' \quad (46)$$

where the term standing for the given reference points in Eq.(46) is

$$R_n^E = \sum_{k=1}^{m(n)} \frac{P_n^E}{Q_n^E} \quad (47)$$

with

$$P_n^E = (z_n' - z_{n,1})\cdots(z_n' - z_{n,k-1}) * *(z_n' - z_{n,k+1})\cdots\left(z_n' - z_{n,m(n)}\right) \quad (48)$$

and

$$Q_n^E = (z_{n,k} - z_{n,1})\cdots(z_{n,k} - z_{n,k-1}) * *(z_{n,k} - z_{n,k+1})\cdots\left(z_{n,k} - z_{n,m(n)}\right) \quad (49)$$

For the other parameters and variables the same expressions alike (45) and (46) can be introduced and the design values at arbitrary locations in the flowfield may possibly be given. Using discretized expressions for (45), (46) and the others, we can numerically find the locations of the reference points. Consequently, we may feasibly use the direct solutions in designings.

Numerical Examples

Consideration of the questions of existence, uniqueness, stability and construction in a complete solution of inverse problems, is of great importance in testing the assumption behind any mathematical model. Here the present inverse method demonstrates the ideal cases in which the data are supposed to be known exactly and complete. Using the calculated results for the unsteady inlet transonic rotor flow [1] and the linear cascade flows with and without air-injection[2], the numerical examples to reconstruct the suction surfaces are shown. Since the computation paths for the direct and inverse solvers, as shown in Fig. 3, coincided or were parallel with each other, the informations could be easily interchanged between the solvers. In Fig. 4, the computation paths shown with broken lines on the different cross-sectional computation surfaces in a blade passage were to be reconstructed. Nine sheets of cross-sectional computation surfaces were arranged in a blade passage and hundred reference points standed for a suction side profile section to be designed on a blade-to-blade computation surface. Both codes were written in FORTRAN for a HITAC S3800/480 and are applicable to unsteady three-dimensional transonic rotor flow calculations. They proved useful for the practical cases.

Unsteady Inlet Transonic Rotor Flow

A numerical result to stress on the important roles of the unsteadiness and nonuniformity detected at the inlet, was given for the axial transonic flow through the 23 bladed overhung rotor without inlet guide vanes installed in MIT Blow Down Facilities[1]. In the computation of the result[1], reflecting the experimental circumstances, some simplifications such as Prandtl number of 1.0 and the sinusoidal oscilation of the inlet Mach number with 2.5 percent of an amplitude of deviation, were assumed without loss of generality. The tip clearance effect was omitted for the simplification of the computation. The experimentally supposed conditions such as the tip relative Mach number of 1.30, radially constant stagnation temperature rise, uniform inlet conditions and the shockless through flow, were also introduced.
For the reconstruction of profile contour, we assumed that the pressure sides of different profile sections were fixed and only the suction sides were flexible, except for the sections at hub and tip. Fig. 5 (a) and (b) show the first approximations of the profile sections on the suction side near at the tip and at the hub, respectively. The original blade contour was constructed, using 6 cross sections from the hub to the tip and the hub ratio was 0.5 at the leading edge. For the modification of blade thickness the adjacent blade section was referred and 30 percent of the differnce in thickness between the sections was added or subtracted to the original thickness. The code in the direct problem, for the non-uniform case, consumed a memory of about 600 Mega bites as working volume and approximately 3 hours of CPU time[1]. Using the detailed results from the direct problem, the current run of inverse code for the reconstruction required 100 Mega bites and about 15 minutes of CPU time, additionally. To check the sensitivity of soltion to the given data set and to errors in it, the same code was applied to a conventionally transformed cascade geometry shown in Fig. 6 for the reconstruction of the pressure side. The contours on pressure side at different sections resemble each other for this case. Fig. 7 shows the original profile contour and its first approximation in the run. Using the given data and the first approximations, the code also reconstructed the original profile with five digits. For this case CPU time of approximately 10 minutes was required.

Linear Cascade Flows With and Without Air-Injection

The other numerical result to show the matching between the non-uniformity at the inlet and the assumed velocity distributions of film-cooling inflows[2] was also used. Fig. 8 shows the original profile contour and the location of the slit. According to the experimental data, the result was calculated for a linear cascade in an annular flowfield under the simplified condition that the injected air and the main stream were at room temperature and the radially varied but azimuthally uniform total pressure loss distribution at the inlet, were assumed[2]. The test Reynolds number based on the mass-averaged cascade outlet and the blade chord was about 1.5×10^5 and the test incidence at the mid span was -2.8 degrees. The calculated total pressure loss distribution maps without and with air-injection were plotted with 10 percent intervals, in Figs. 9 and 10, respectively. For both cases the same first approximation of profile contour on the suction surface shown in Fig. 8 was used. The profile was given such that 20 percent of additional thickness was added to the original suction surface and the pressure surface profile was unchanged. Employing the given results from the direct solution and the first approximation, the above mentioned code was applied to the flowfields without and with air-injection. The reconstruction of the original profile was successfully done both without and with air-injection cases. For the direct problem the code required a memory of about 400 Mega bites as working volume and approximately 20 minutes of CPU time. For the inverse calculation additional 80 Mega bites as working volume was necessary. For both cases the additional 10 minutes of run gave the converged results with five digits of accuracy.

Conclusions

An inverse-direct hybrid Navier-Stokes solver using pseudo-analytic function theories, which can deal with objectives of everyday designings in engineering, is presented. The incorporation and interchange of necessary informations between direct and inverse methods can be smoothly and completely done. The present paper stressed on the ideal cases with the perfect data. The application of present method to a conventional designing of blade contours was very easy and could be done completely. The numerical examples to reconstruct the blade suction surfaces for the unsteady inlet transonic rotor flow and the linear cascade flows without and with air-injection, were successfully shown. The stabilities in inverse computations for both cases were very good and the code proved useful for the cases.

References

(1)Miyazaki,T., "An Approach to Numerical Experiments for Arbitrary Inlet Conditions in 3D Compressible Viscous Cascade Flows," 19th Congress of the International Council of the Aeronautical Sciences, Vol.2, ICAS-94-6.5.3, Sept. 1994, 1718-1727.

(2)ibid., "An Application of the Navier-Stokes Solver with Pseudo-analytic Functions to Film-Cooling Flowfields," 6th International Symposium on Computational Fluid Dynamics, Sept. 1995, Lake Tahoe, USA, 839-844.

(3)ibid., "Numerical Analysis of 3D Compressible Cascade Flows with Arbitrary Inlet Condition Using the Navier-Stokes Solver Based on Pseudo-analytic Functions," Computational Fluid Dynamics Journal, Vol.3, No.3, Oct. 1994, 379-394.

(4)ibid., "A Theoretical Solution of the Unsteady Three-Dimensional Compressible Navier-Stokes Equation by Pseudo-analytic Function Theories :An Application to Arbitrary Turbomachines," Proc. of the 2nd Japan-Soviet Union Joint Symposium on Computational Fluid Dynamics, August 1990, Tsukuba, Japan, Vol. 1, 235-251.

(5)Colton, D.L., Solution of Boundary Value Probblems by the Method of Integral Operators, Pitman Pub., 1976.

(6)Vekua, I.N., Generalized Analytic Functions, Pergamon Press, London, 1962.

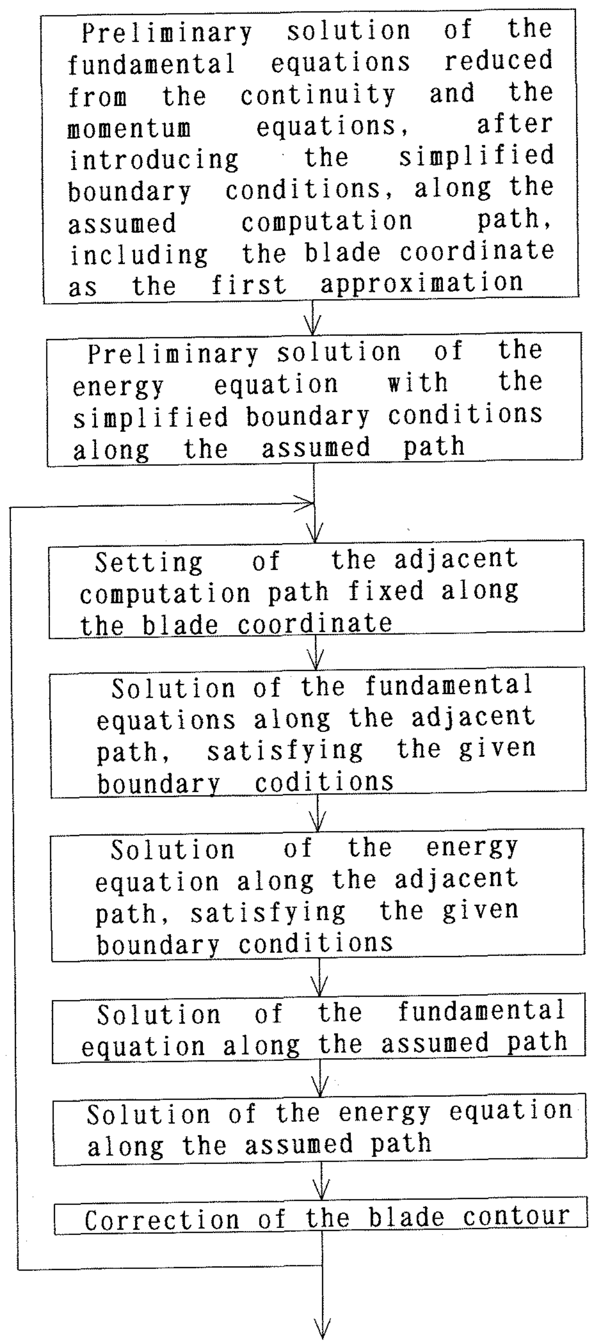

Fig. 1 Scheme for designing of the blade contour

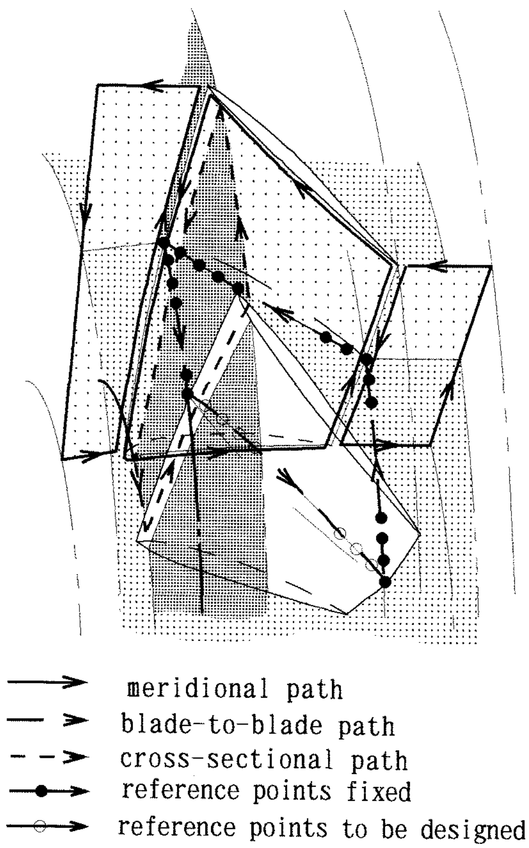

Fig. 2 Computation paths

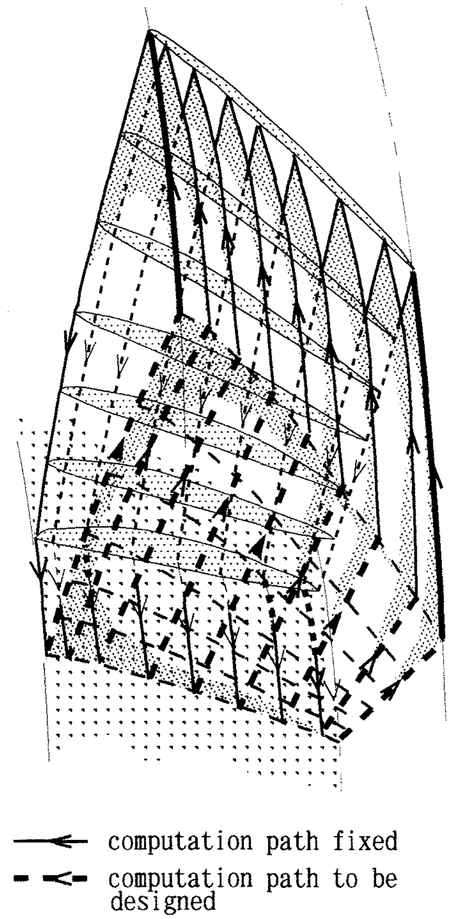

Fig. 4 Cross-sectional surfaces and computation paths

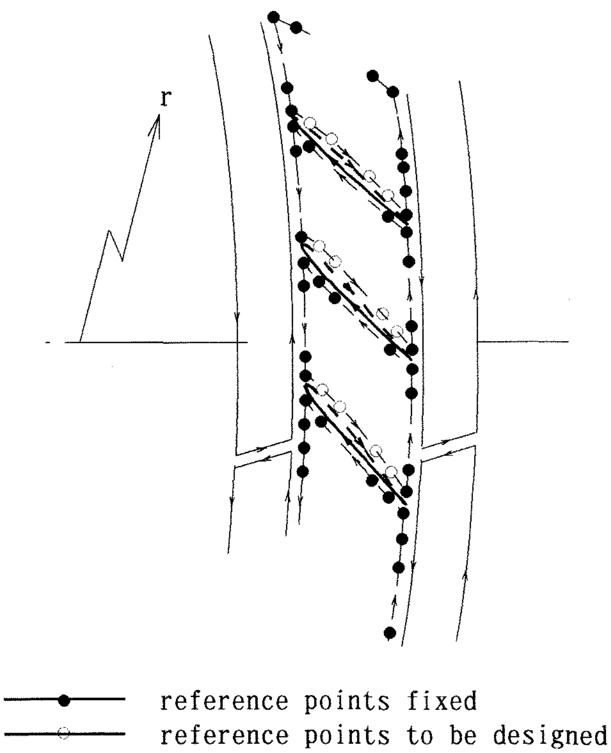

Fig. 3 Computatin paths on a blade-to-blade surface

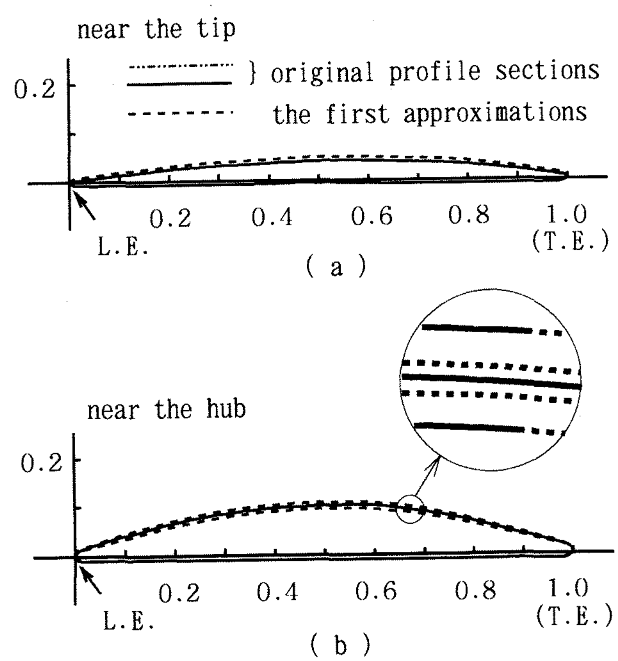

Fig. 5 Reconstruction of profile sections

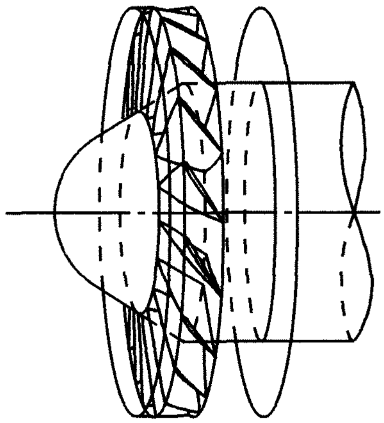

(a) Existing cascade geometry

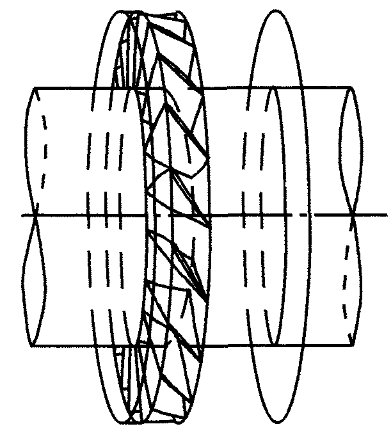

(b)Transformed cascade geometry

Fig. 6 Transformation of flowfield

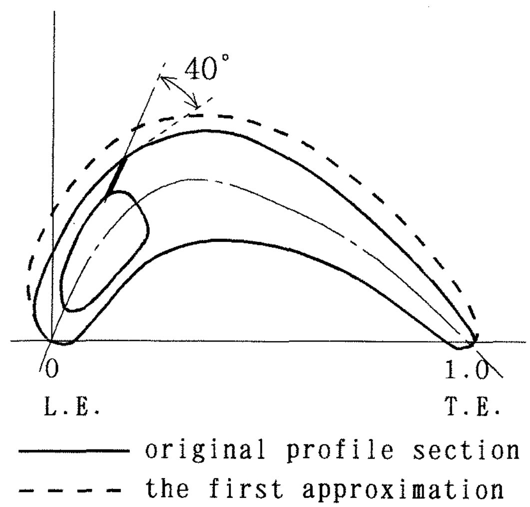

Fig. 8 Reconstruction of blade contour with air-injection

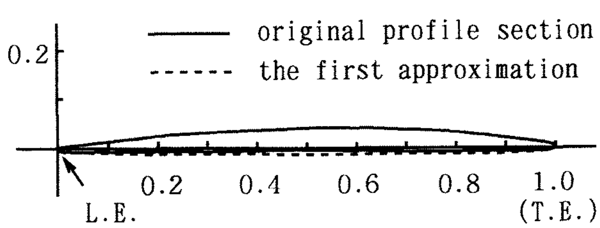

Fig. 7 Reconstruction of profile section on pressure side

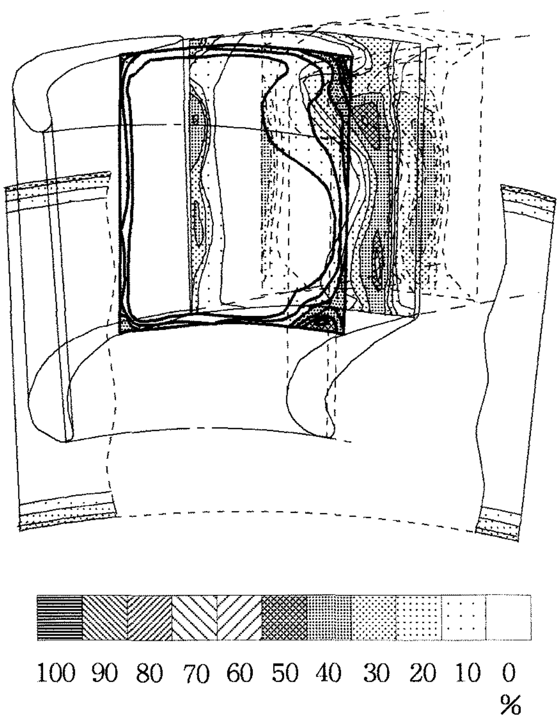

Fig. 9 Total pressure loss maps (without air-injection)

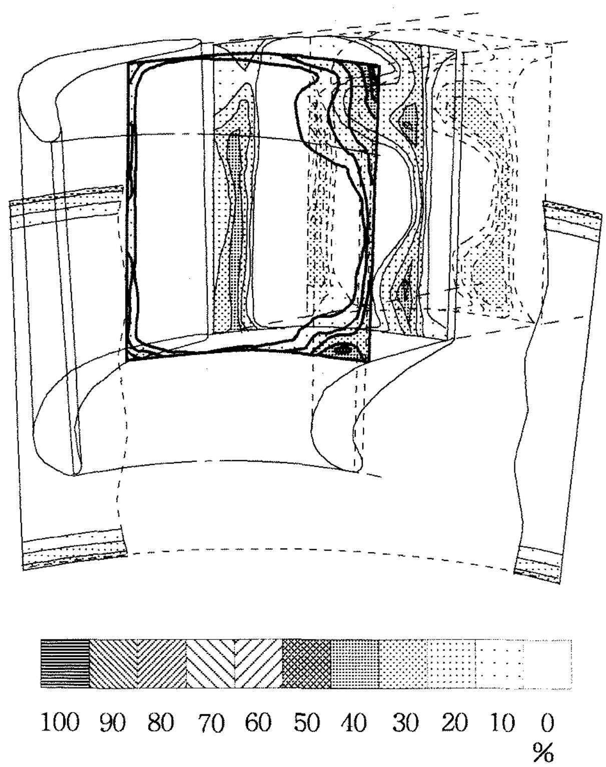

Fig. 10 Total pressure loss maps (with air-injection)